NEUROSCIENCE
RESEARCH ARTICLE

INTERNATIONAL BRAIN IBRO RESEARCH ORGANIZATION

Abraham J. Cisneros-Mejorado et al. / Neuroscience xxx (2019) xxx–xxx

Demyelination–Remyelination of the Rat Caudal Cerebellar Peduncle Evaluated with Magnetic Resonance Imaging

Abraham J. Cisneros-Mejorado, Edith Garay, Juan Ortiz-Retana, Luis Concha, Juan P. Moctezuma, Samuel Romero and Rogelio O. Arellano*

Instituto de Neurobiología, Universidad Nacional Autónoma de México, Boulevard Juriquilla 3001, Juriquilla Querétaro, CP 76230, Querétaro, Mexico

**Abstract—Remyelination is common under physiological conditions and usually occurs as a response to a pathological demyelinating event. Its potentiation is an important goal for the development of therapies against pathologies such as multiple sclerosis and white matter injury. Visualization and quantification *in vivo* of demyelination and remyelination processes are essential for longitudinal studies that will allow the testing and development of promyelinating strategies. In this study, ethidium bromide (EB) was stereotaxically injected into the caudal cerebellar peduncle (*c.c.p.*) in rats to produce demyelination; the resulting lesion was characterized *(i)* transversally through histology using Black-Gold II (BGII) staining, and *(ii)* longitudinally through diffusion-weighted magnetic resonance imaging (dMRI), by computing fractional anisotropy (FA) and diffusivity parameters to detect microstructural changes. Using this characterization, we evaluated, in the lesioned *c.c.p.*, the effect of N-butyl-β-carboline-3-carboxylate (β-CCB), a potentiator of GABAergic signaling in oligodendrocytes. The dMRI analysis revealed significant changes in the anisotropic and diffusivity properties of the *c.c.p.* A decreased FA and increased radial diffusivity ($\lambda_\perp$) were evident following *c.c.p.* lesioning. These changes correlated strongly with an apparent decrease in myelin content as evidenced by BGII. Daily systemic β-CCB administration for 2 weeks in lesioned animals increased FA and decreased $\lambda_\perp$, suggesting an improvement in myelination, which was supported by histological analysis. This study shows that structural changes in the demyelination–remyelination of the caudal cerebellar peduncle (DRCCP) model can be monitored longitudinally by MRI, and it suggests that remyelination is enhanced by β-CCB treatment.*This article is part of a Special Issue entitled: SI: Miledi's contributions.*

Key words: OPC, diffusion tensor imaging, white matter, GABAergic signaling, β-carbolines.

INTRODUCTION

Myelination is critical for fast and efficient communication among neurons in the nervous system. Damage that compromises the normal myelination process in the central nervous system (CNS) produces demyelinated axons that undergo swelling and neural degeneration (Kassmann and Nave, 2008). Several neurological disorders are related to white matter and lead to hypomyelination and axonal dysfunction (Cammer and Zhang, 1999; McGavern et al., 1999; Perry and Anthony, 1999; Trapp et al., 1999; Van der Valk and De Groot, 2000; De Stefano et al., 2001). In some cases, after demyelination, the adult brain is able to generate new myelin through remyelination in the lesioned regions (e.g., Woodruff and Franklin, 1999; Fancy et al., 2004; Zhao et al., 2008; Gautier et al., 2015). A comprehensive understanding of remyelination could be useful to generate new therapeutic tools. In fact, several *in vivo* experimental models have been developed to study the biology of this important healing process.

To produce experimental demyelination, researchers have used models based on the local or general administration of autoreactive antibodies against myelin components (e.g., experimental autoimmune encephalomyelitis; Raine et al., 1974; Meeson et al., 1994; Dal Canto et al., 1995); they have also used viral infection tools (e.g., Godfraind et al., 1989; Miller and Rodriguez, 1996) and generated local lesions by thermal injury (Sasaki and Ide, 1989) or toxin administration (e.g., ethidium bromide or lysolecithin; Blakemore, 1974; Matute, 1998; Woodruff and Franklin, 1999). In general, after a demyelinating episode, a well-orchestrated

*Corresponding author at: Instituto de Neurobiología, Universidad Nacional Autónoma de México, Boulevard Juriquilla 3001, Juriquilla Querétaro, CP 76230, MÉXICO. Tel.: +52-5556234062.
E-mail address: arellano.ostoa@comunidad.unam.mx (Rogelio O. Arellano).

Abbreviations: c.c.p., caudal cerebellar peduncle; *s.v.n.*, spinal vestibular nucleus; EB, ethidium bromide; dMRI, diffusion-weighted magnetic resonance imaging; DTI, diffusion tensor imaging; FA, fractional anisotropy; PDV, principal diffusion vector; OPC, oligodendrocyte precursor cell; CtxN, cortical neurons; β-CCB, N-butyl-β-carboline-3-carboxylate; BGII, Black-Gold II; ROI, region of interest.

https://doi.org/10.1016/j.neuroscience.2019.06.042
0306-4522/

regenerative process is initiated; however, the array of signaling events involved in the phenomenon has yet to be fully understood (Fancy et al., 2011). Remyelination *in vivo* is often incomplete, and a degree of chronic demyelinated lesions persists (Wolswijk, 1998). Systematic and accurate assessments of these conditions (i.e., demyelination–remyelination) *in vivo* could be highly beneficial to evaluate and develop novel therapeutic strategies.

An important addition to these models would be to combine a longitudinal analysis strategy with the use of specific pharmacological tools to assess *in vivo* the possible effects of drugs and monitor the (re)myelination time-course and its efficiency. The non-invasive and innocuous nature of magnetic resonance imaging (MRI) affords this approach. Moreover, diffusion-weighted MRI (dMRI) and its analysis through mathematical models allow a suitable delineation of white matter structures and the evaluation of its myelination in subjects under pharmacological treatment at different stages. The displacement of water molecules is modulated by the biological barriers they encounter at the mesoscopic level (e.g., axonal membranes, myelin sheaths) (Beaulieu, 2002). Therefore, water self-diffusion is not free, and the analysis of the three-dimensional diffusion profile yields information about tissue microstructure (Concha, 2014). Diffusion tensor imaging (DTI; Basser et al., 1994) provides a mathematical framework to analyze dMRI and can be used to infer changes in myelination. Fractional anisotropy (FA) is a unit-less DTI-derived metric that quantifies the amount of directionality that water diffusion shows in a particular imaging region (voxel) and is low (zero) when water diffuses freely, and high (maximum of one) in highly organized tissue with several spatially coherent tissue boundaries. In the nervous system, demyelination alters the microstructure and reduces FA in white matter structures with a single axonal population. This parameter correlates with the induced damage and has been used extensively in clinical studies to characterize changes related to damage in the white matter (e.g., Yurgelun-Todd et al., 2007; Stricker et al., 2009; Li et al., 2010; Bora et al., 2011; Rodríguez-Cruces et al., 2018). Also, FA analysis has been used in experimental models to detect alterations in myelin (e.g., Song et al., 2002; Song et al., 2003; Larvaron et al., 2007; Fatemi et al., 2009; Boretius et al., 2012). The development of a non-invasive and standard method in mammals to differentiate and monitor axonal and myelin damage *in vivo* could be useful for experimental pharmacological approaches to modulate the myelination process.

In this study, we applied dMRI to provide information on the degree of FA change produced in the demyelination–remyelination of the caudal cerebellar peduncle (DRCCP model; Woodruff and Franklin, 1999), and we correlated the changes with histological Black–Gold II (BGII) staining. The *c.c.p.* tract is especially suitable for monitoring its structure because it is densely myelinated with large-diameter axons projecting in parallel orientation (Woodruff and Franklin, 1999), thus providing dMRI images that can be evaluated with a high degree of robustness and allowing *in vivo* analysis of its microstructure. In addition, since GABAergic signaling has been recently proposed to contribute to myelination (Zonouzi et al., 2015; Arellano et al., 2016; Hamilton et al., 2017), we tested the pharmacological effect of GABAergic signaling potentiation on remyelination. For this purpose, we analyzed the effect of administering N-butyl-β-carboline-3-carboxylate (β-CCB), a suggested endogenous β-carboline (Peña et al., 1986) that has a positive allosteric modulator effect on the $GABA_A$ receptor expressed in oligodendrocytes (Arellano et al., 2016). The results indicated that demyelination and remyelination can be monitored and evaluated by DTI analysis, and that β-CCB administration accelerated recovery of DTI metrics, suggesting a remyelination improvement supported by BGII histological analysis.

EXPERIMENTAL PROCEDURES

Study Approval

All experiments were performed by trained personnel and conducted in accordance with the Ethics Committee of the Instituto de Neurobiología of the Universidad Nacional Autónoma de México. The *in vivo* experiments were conducted with male Sprague–Dawley (SD) rats (280–310 g, 10–12 weeks) in accordance with the Guide for Care and Use of Laboratory Animals (National Institutes of Health). All possible efforts were made to comply with 3R standards and minimize animal suffering and the number of animals used.

Demyelination and remyelination of caudal cerebellar peduncle (DRCCP)

The demyelinating lesion was induced as previously described (Woodruff and Franklin, 1999). Rats were anesthetized with ketamine/xylazine (a mixture of 70 mg/kg and 6 mg/kg, respectively, dissolved in saline solution) and then positioned on a stereotaxic instrument (Stoelting Co., Wood Dale, IL, USA) in a surgery room at room temperature (RT). Demyelination was induced by injecting 2 μL of 0.05% ethidium bromide (EB) into the caudal cerebellar peduncle (*c.c.p.*) of male rats in accordance with the Paxinos atlas (Paxinos and Watson, 2007) as follows: AP −2.28 mm (from interaural), LR 3.2 mm (from midline), H 7.6 mm, and the incisor bar positioned 3.5 mm below the center of the aural bars. Surgery control animals were injected with an equal volume of sterile saline solution. After the surgical procedure, animals were left in the surgery room for 1–3 h to monitor the neurological condition caused by the trauma.

At the time of the experiments, animals were divided into two main groups: 1) the non-lesioned group (injected with saline solution) and 2) the lesioned group (injected with EB in solution). For histological evaluation of myelin, the non-lesioned group was of 9 animals, 5 were processed for coronal slices and 4 for sagittal preparations, while the lesioned group also included the subgroups named β-CCB treated (n = 11 animals, 5 coronal and 6 sagittal) and the β-CCB untreated (n = 10 animals, 5 coronal and 5 sagittal). For experiments *in vivo*, the main groups, lesioned and non-lesioned, were subdivided in the β-CCB untreated (n = 8, 4

lesioned and 4 non-lesioned) and the β-CCB treated subgroups (n = 8, 4 lesioned + β-CCB treated and 4 non-lesioned + β-CCB treated).

Black–Gold II (BGII) and Luxol fast blue histochemistry for myelin

For histological examination, rats were transcardially perfused with 0.1 M phosphate buffer (pH 7.2) followed by 4% paraformaldehyde (PFA) in the same buffer. After extraction, brains were maintained overnight in PFA. Then, the tissue was cryoprotected in 25% sucrose at 4 °C for at least 24 h. Coronal (30 μm) or sagittal (40 μm) cryosections were cut and mounted on electrocharged slides and stored at −20 °C until staining with the BGII compound (EMD Millipore Corp., Billerica, MA, USA), as previously described (Schmued et al., 2008). Briefly, tissue sections were rehydrated in distilled water for about 2 min at RT. Then, slides were transferred to a 0.3% BGII solution dissolved in 0.9% saline vehicle (NaCl) and heated to 60–65 °C. Preparations were monitored every 5 min until reaching the desired degree of staining with BGII. Next, the slides were rinsed for 2 min in distilled water, transferred to a 1% sodium thiosulfate solution for 3 min at 60–65 °C, and rinsed two or three times with distilled water. For the Nissl counterstaining, the slides were transferred to a solution of 0.1–0.2% cresyl violet (blue; EMD Millipore Corp., Billerica, MA, USA) in 0.1% acetic acid for 5 min and then rinsed two times with distilled water. After, the tissue was dehydrated using sequential graduated alcohol solutions (50, 70 and 96%) and immersed in xylene for 1 min. The slides were then coverslipped with Permount mounting medium. For Luxol fast blue (LFB) stain, coronal cryosections were cut at 5 μm then mounted onto electrocharged slides and hydrated in distilled water and immersed in ethanol (first in 70% and after 90%). The preparations were incubated overnight with 0.1% LFB at 60 °C then washed twice with ethanol for 2 min. Next, slides were immersed in xylene for 1 min and coverslipped with the mounting media. For myelinated zone assessment, tissue sections for BGII were visualized and analyzed under a microscope, and representative images were acquired with a Leica ICC50 HD camera (Leica Microsystems, Wetzlar, Germany). Optical density of myelin BGII staining in selected brain areas from *c.c.p.* was quantified using ImageJ software (version1.52i). Briefly, after converting the images to grayscale, optical intensity was obtained from a given region of interest (ROI) of the *c.c.p.* Optical density was calculated by normalizing intensity values from each *c.c.p.* ROI against the background intensity value from each section (Hakkarainen et al., 2016), applying the following relationship: (intensity of background − mean intensity of labeling in ROIs)/intensity of background. Then, in coronal slices, the ipsilateral optical density was expressed as the percentage relative to its contralateral side. For sagittal slices, the ipsilateral optical density of *c.c.p.* was normalized with respect to that obtained from the spinal vestibular nucleus (*s.v.n.*), a non-lesioned tract located just below the *c.c.p.* (Fig. 5).

Magnetic resonance

Anesthesia was induced with isoflurane (4%, compressed air) using an anesthetic chamber and maintained under 1–2% (compressed air) with a facemask during the procedure. T2-weighted imaging and dMRI were performed at the National Laboratory for Magnetic Resonance Imaging using a 7-T magnet (Bruker Pharmascan 70/16US). Data sets for DTI were acquired using a spin-echo, single-shot echo-planar imaging sequence with the following parameters: slice thickness = 0.65 mm, no inter-slice gap, no physiological gating, TR = 2 s, TE = 26 ms, FOV = 25 × 25 mm, image size = 167 × 167 mm, resolution = 150 × 150 mm, 64 diffusion directions, b = 650 s/mm^2, 1 average. T2-imaging was acquired with the following parameters: slice thickness = 0.5 mm, no inter-slice gap, TR = 2.5 s, TE = 33 ms, FOV = 30 × 20 mm^2, image size = 250 × 170 mm^2, resolution = 120 × 118 mm^2, 9 averages and 22 slices. Pre-processing of dMRI data sets included both reduction of motion and eddy current-induced geometric distortions by linear transformation of each volume to the average non-diffusion weighted volume and denoising via random matrix theory (Veraart et al., 2016). Total scan time was 36 min per animal. The MRtrix software package (http://www.mrtrix.org) was used to estimate the tensor model, from which we derived fractional anisotropy (FA) maps, principal diffusion vector (PDV), and radial and axial diffusivities ($\lambda_{\perp}$ and $\lambda_{||}$, respectively). DTI parameters were analyzed using ROI analysis. ROIs of the *c.c.p.* were manually delineated on PDV images. Sixteen animals, four groups of four animals each, as described above, underwent this scanning protocol; first before lesioning and then every week from 14 until 35 days post-lesion (dpl).

Cortical neuronal culture preparation

Primary cultures of cortical neurons (CtxN) were established in accordance with previously described procedures (Larm et al., 1996). Briefly, neurons derived from cortical lobes of Wistar rat embryos (E18) were isolated and digested in Hank's balanced salt solution (Gibco; Thermo Scientific, Waltham, MA) containing 0.25% trypsin and 0.4% DNase. A dissociation was made with needles (21G, 23G, 25G), centrifuged and resuspended in B27 neurobasal medium (Gibco; Thermo Scientific, Waltham, MA) plus 10% Fetal Bovine Serum (FBS; Hyclone, Thermo Scientific, Waltham, MA) and seeded at 1 × 10^5 cells per well onto poly-L-ornithine-coated 24-well plates bearing coverslips with a 12-mm diameter. Twenty-four hours later, this medium was replaced by serum-free medium containing B27 plus antibiotic-antimycotic and glutamine (2 mM). Cultures were maintained at 37 °C and 5% CO_2; recordings were made in neurons from four different cultures maintained from 10 to 14 days *in vitro*.

Oligodendrocyte precursor cell (OPC) cultures

First, a primary mixed glial culture was prepared in accordance with the modified method of McCarthy and de Vellis (1980). Briefly, cortices were isolated from forebrains and digested by incubation (15 min, 37 °C) in Hank's balanced salt

solution containing 0.25% trypsin and 0.4% DNase. Dissociation was made with needles (21G, 23G), centrifuged, and resuspended in Iscove's modified Dulbecco's medium supplemented with 10% FBS and antibiotic–antimycotic solution. Cells were seeded onto poly-D-lysine-coated flasks (75 cm^2) and maintained in culture at 37 °C and 5% CO_2. After 10 days in culture, the flasks were shaken (400 rpm for 2 h at 37 °C) to remove loosely adherent microglia. The remaining OPCs were dislodged by shaking overnight at 400 rpm. The cell suspension was then filtered through a 10-μm nylon mesh and preplated on bacterial grade Petri dishes for 2 h in a chemically defined medium (OPC medium; Sánchez-Gómez et al., 2018) consisting of Dulbecco's modified Eagle's medium supplemented with 100 μg/mL transferrin, 60 ng/mL progesterone, 40 ng/mL sodium selenite, 5 μg/mL insulin, 16 μg/mL putrescine, 100 μg/mL BSA. Cells were plated onto poly-D-lysine-coated 12-mm-diameter coverslips in 24-well culture dishes at a density of 5×10^3 cells per well and cultured in the presence of the mitogenic factors PDGF-AA (5 ng/mL) and bFGF (5 ng/mL) to expand their number and prevent their differentiation. After 1 day in culture, OPCs represented >95% of the total cells as assessed by immunocytochemistry (Arellano et al., 2016). Recordings were made in OPCs from five different cultures maintained from 1 to 2 days *in vitro*.

Electrophysiology

Whole-cell patch-clamp recordings of ionic currents of both CtxN and OPCs were performed using the Axon 200B patch-clamp amplifier (Axon Instruments; Sunnyvale, CA, USA). Currents were regularly recorded at a holding membrane potential of −80 mV. Neurons or OPCs were constantly perfused with external solution containing (in mM) 140 NaCl, 3 KCl, 1 $CaCl_2$, 1 $MgCl_2$ and 10 HEPES, adjusted to pH 7.4 (NaOH). Patch-clamp pipettes (3–5 MΩ) were filled with internal solution adjusted to pH 7.4 (KOH) containing (in mM) 130 KCl, 5 NaCl, 2 EGTA, 1 $MgCl_2$, 2 Mg-ATP, 0.2 Na-GTP and 10 HEPES. Recordings were acquired and digitized with a Digidata 1440 (Molecular Devices, Sunnyvale, CA, USA) and analyzed with pClamp software (v.10; Molecular Devices) (Arellano et al., 2016; Pérez-Samartín et al., 2017).

β-carboline administration

For *in vivo* administration of β-carboline, the vehicle as control or β-CCB solution was prepared in aliquots and then coded alphanumerically by an independent researcher. The preparations of β-CCB were made daily before the injection, similar to methods used for other β-carbolines elsewhere (e.g., Grella et al., 1998; Farzin and Mansouri, 2006). Briefly, β-CCB (1 mg/Kg) was mixed in vehicle containing sterile phosphate-buffer salts (PBS 1×, 70% *v*/v) and sunflower seed oil (30% v/v) for a final volume of 200 μL. The mixture was sonicated for 60 min at 37 °C. Vehicle alone or β-CCB solution was administered by intraperitoneal (i.p.) injection after 14 days of *c.c.p.* injection with either EB or saline solution; this was done every 24 h from day 14 until day 28. Treatment with β-CCB for the time and doses indicated did not cause obvious changes in animal behavior, such as open-field exploration, freezing or signs of pain, anxiety or apparent aggression, and the animals' exploration of the environment was normal. Finally, rats were randomly assigned to each treatment on the basis of a blinded analysis.

Substances

N-butyl-β-carboline-3-carboxylate (β-CCB) was obtained from Tocris Bioscience (Bristol, UK), isoflurane from PiSa Lab (PiSa, Guadalajara, JAL, México), and Permount mounting medium from Fisher Scientific (FS, Fair Lawn, NJ, USA). All other salts, PFA, GABA, EB, acetic acid, sunflower seed oil, poly-L-ornithine, poly-D-Lysine and xylenes were acquired from Sigma-Aldrich.

Statistical analysis

All data are expressed as mean ± S.E.M. The means of two groups were compared using a Student's t-test or, when appropriate, an analysis of variance followed by post-hoc comparisons of individual means using the Fisher correction. Statistical analysis was performed using GraphPad Prism software. Differences were considered to be significant at $P < 0.05$.

RESULTS

The caudal cerebellar peduncle analyzed using BGII and MRI

The *c.c.p.* tract has been chosen as an area of injury and remyelination analysis because of its characteristics, as detailed since the implementation of this model (Woodruff and Franklin, 1999; see also, Fancy et al., 2004; Gautier et al., 2015). Here, the *c.c.p.* was examined using two modern techniques: BGII staining and MRI. BGII staining (Schmued et al., 2008) colored myelinated tracts red to brownish (Fig. 1, second row) in proportion to the amount of myelin. The *c.c.p.* presents a characteristic drop-like shape observed at −11.04 mm from bregma, according to the Paxinos atlas (Paxinos and Watson, 2007; Fig. 1, top row), and can be followed in contiguous slices (Fig. 1 also illustrates slices at −10.08 mm and −11.64 mm from bregma). On the other hand, when using dMRI, although T2-weighted images in coronal slices had good quality, their contrast was insufficient to localize the intact *c.c.p.* (Fig. 1, third row), however, the *c.c.p.* was conspicuous on FA and PDV maps (Fig. 1, bottom two rows).

White matter injury in the *c.c.p.* (DRCCP model)

A structural analysis using both BGII and MRI techniques was made at 35 days' post lesion (dpl) after 2 μL EB (0.05%) injection at the coordinates corresponding to the *c.c.p.* Images obtained with both techniques suggested a significant decrease of *c.c.p.* myelin; these hypomyelinated areas were observed up to 6 weeks after the injection, which is consistent with previous reports using electron microcopy techniques (Woodruff and Franklin, 1999). For

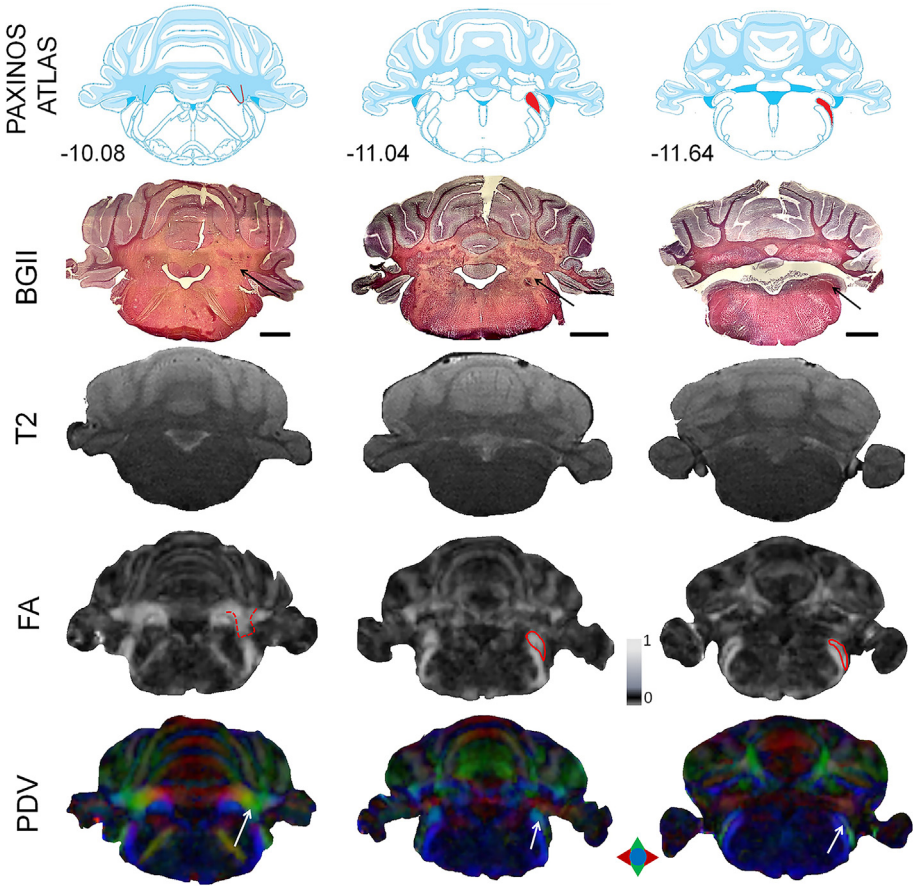

Fig. 1. Caudal cerebellar peduncle detection by BGII and MRI. Upper row diagrams are coronal drawing sections based on the Paxinos atlas illustrating the caudal cerebellar peduncle (*c.c.p.*, red areas). Each section (column) was taken at −10.08 mm, −11.04 mm and −11.64 mm from bregma, respectively. The second row shows similar sections where the tissue was stained with BGII and counterstained with Nissl's stain. The *c.c.p.* location is indicated by black arrows (bar = 2 mm). The following rows correspond to maps derived from MRI analysis as indicated: T2-weighted image (T2); fractional anisotropy (FA) map; and principal diffusion vector (PDV). In FA and PDV, the *c.c.p.* area is indicated by red lines and arrows, respectively. Scales in this and following figures: FA, 0–1 as black–white; PDV, red for left–right, green for dorso-ventral, and blue for rostral–caudal direction.

example, the histological evaluation with BGII at 35 dpl showed a decrease in staining intensity when comparing the injected *c.c.p.* and the contralateral *c.c.p.* in the same slice (n = 5; Fig. 2A–B); this decrease was quantified estimating the optical density in the BGII-stained preparations (Fig. 4E). In sagittal sections, *c.c.p.* lesions also appeared as areas with a decreased optical density (n = 5; Fig. 5). Another technique commonly used to identify changes in myelin content is LFB staining (e.g., Schmued, 1990; Kutzelnigg et al., 2005). Slices processed with this technique also showed a lower intensity of staining in the EB-injected *c.c.p.* than in the contralateral non-lesioned side (n = 4; Fig. 2C–D).

Using MRI, we built and analyzed structural maps to correlate possible changes in white matter with an EB-induced alteration. First, T2-weighted images showed a hyperintense area (red arrow in Fig. 2E) ipsilateral to the EB injection site and at the *c.c.p.*; this was important, as it provided a way to quickly confirm the correct application of EB. FA maps (Fig. 2F) showed reduced values in the area corresponding to the *c.c.p.*, as confirmed in the PDV maps (Fig. 2G). ROIs of the *c.c.p.* were drawn on the PDV maps to quantify the FA from both ipsilateral and contralateral sides to the lesion. The EB injection caused a decrease in FA of about 15% (FA = 0.49 ± 0.04, and 0.42 ± 0.02, for contralateral and ipsilateral, respectively; n = 4 for each case). As previously shown (Arfanakis et al., 2002; Kumar et al., 2009), an FA decay suggests a correlation with a decrease in myelination at the lesioned *c.c.p.* This finding supports the idea that the proposed histological and imaging techniques can be used for longitudinal studies in the DRCCP model.

Effect of β-CCB treatment on the DRCCP model evaluated by BGII and MRI

One of the main objectives of this work was to determine whether the described structural analysis might be useful to assess the possible effects of drugs on myelination or remyelination. Here, the effect of a β-carboline was evaluated in the DRCCP model using BGII and MRI techniques. A previous study showed that β-CCB acted as a positive allosteric modulator on the $GABA_A$ receptor expressed in OPCs or oligodendrocytes maintained *in vitro* (Arellano et al., 2016). This differed from the original description that β-CCB (and other β-carbolines) acted as an inverse agonist by decreasing the $GABA_A$ response in neurons and displaying opposite effects to those shown by benzodiazepines. Here, we confirmed that β-CCB distinguished between the $GABA_A$ receptors expressed in either OPCs or CtxN maintained *in vitro*. As shown in Fig. 3, GABA responses were monitored in each cell type under two conditions: the absence or presence of 10 μM β-CCB. GABA responses were generated applying GABA near its respective EC_{10} in each cell type (10 μM and 3 μM for OPC and CtxN, respectively). The GABA-response peak amplitude showed that receptors expressed in OPCs (n = 18) were increased by the co-application with β-CCB (407.8 ± 30.5%, from the control); whereas the responses monitored in neurons (n = 11) were not affected (91.9 ± 8.2%). This result confirmed that β-CCB acted differentially in OPCs and CtxN distinguishing between the $GABA_A$ receptors expressed in these cultured cell types; a characteristic that might be used to potentiate GABAergic signaling in the oligodendroglial lineage.

Taking these data into account, we explored a potential effect of β-CCB on the DRCCP model evaluated by BGII and MRI techniques. First, at 35 dpl, brains from the different

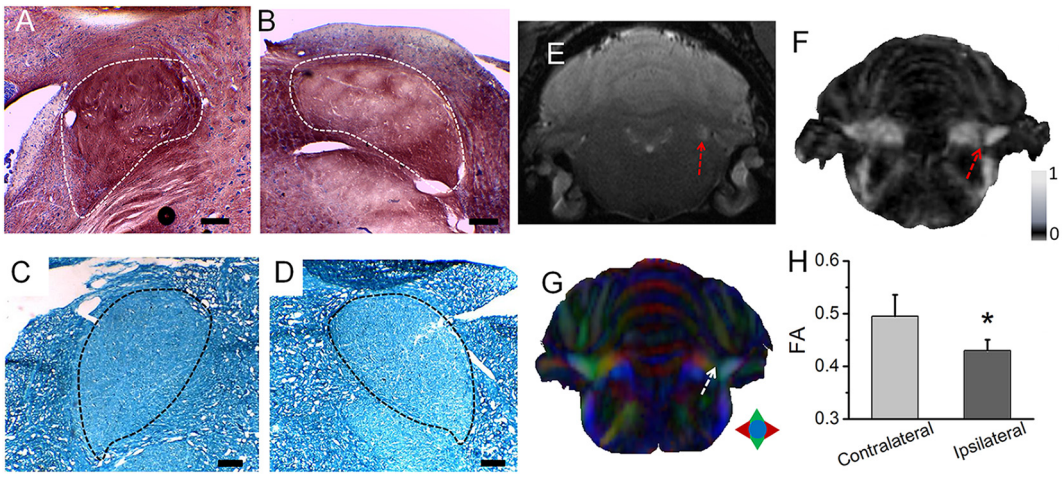

Fig. 2. BGII and MRI techniques allow lesion detection in the DRCCP model. Coronal sections containing the *c.c.p.* (white or black dotted lines) area at 35 dpl, showing both contralateral **(A and C)** and ipsilateral **(B and D)** sides. A–B were stained with BGII, while C–D were processed for Luxol fast blue. **(E)** T2-weighted images at 35 dpl; red arrow signals a hyperintense area at the ipsilateral *c.c.p.* location. **(F–G)** FA and PDV maps also evidence changes in the ipsilateral *c.c.p.* at 35 dpl, whereas the contralateral side remained unaffected. **(H)** Graph shows the value of FA (mean ± S.E.M.) for both contralateral (n = 4) and ipsilateral (n = 4) sides. Bar = 100 μm in A-D. In H, *P < 0.05.

experimental groups were cut, and the BGII technique was applied to either coronal (n = 16) or sagittal (n = 16) preparations. Coronal images from the lesioned group showed a decrease in optical density (to 55 ± 0.03% of control) of BGII staining in the ipsilateral versus the corresponding *c.c.p.* contralateral area, whereas images from the lesioned group treated with β-CCB showed a less pronounced decrease in optical density (to 83 ± 0.06%) in the ipsilateral lesioned side (Fig. 4E). Similar results were obtained from sagittal slices (at 2.62 mm lateral) in which the *c.c.p.* area spanned across a long band (Fig. 5A–B), and images from lesioned animals showed a decrease to 48 ± 0.05% of optical density in BGII-stained *c.c.p.,* with respect to that obtained from the *s.v.n.* in the same slices (Fig. 5 D1–D2, and F); also, images from animals lesioned and treated with β-CCB showed a less pronounced decrease to 89 ± 0.03% in optical density (Fig. 5 E1–E2, and F). In general, a decrease in stain intensity using the BGII technique was detected at around 14 dpl, which was similar to the time-course reported for changes in myelination in the original DRCCP model characterization (Woodruff and Franklin, 1999).

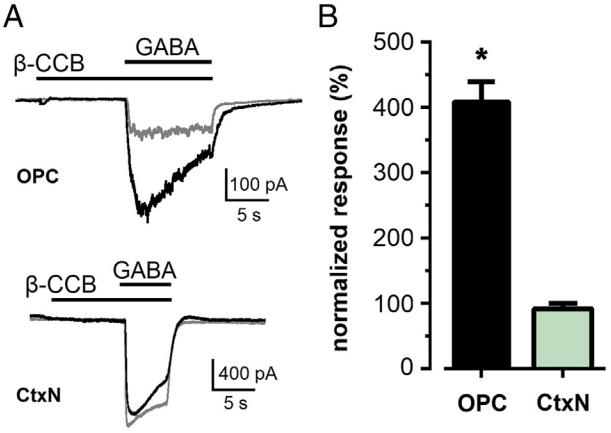

Fig. 3. β-CCB differentially modulated the $GABA_A$ receptor expressed in OPCs and CtxN. **(A)** Traces are responses in OPCs and CtxN elicited by 10 μM and 3 μM GABA, respectively. Each set shows the control GABA response (gray trace) in the absence of β-CCB, and the response to GABA co-applied with 10 μM β-CCB (black trace) in the same cell. **(B)** Graph depicts the normalized current response to GABA in the presence of β-CCB with respect to the control current in OPC (n = 18) and CtxN (n = 11). Histogram shows the mean ± S.E.M.; *P < 0.05, different with respect to the control.

Longitudinal DTI-derived maps were analyzed for both ipsilateral and contralateral sides. FA values for each group are plotted versus time in Fig. 6A–B, and representative maps are illustrated in Fig. 6C–D. In lesioned animals, we observed that FA had substantially decreased by 14 dpl and remained low throughout the analysis period. Lesioned animals treated with β-CCB recovered, reaching FA control values at around 28 dpl. The corresponding contralateral images showed a relatively constant FA value throughout the study (Fig. 6B); in summary, low FA values in the *c.c.p.* of the lesioned group were reverted after 2 weeks of β-CCB treatment. Then, considering the behavior of the DTI maps in the *c.c.p.*, both radial diffusivity ($\lambda_\perp$) and axial diffusivity ($\lambda_{||}$) were also analyzed for the ipsilateral *c.c.p.* for the experiments described in Fig. 6. These parameters reflect tract directionality and are directly related to myelin ($\lambda_\perp$) and axonal ($\lambda_{||}$) damage (Song et al., 2003; Song et al., 2005; Budde et al., 2011). Fig. 7 illustrates the mean values for $\lambda_\perp$ and $\lambda_{||}$ for all the experimental conditions. We observed that in the lesioned group without β-CCB treatment, $\lambda_\perp$ increased more than 35% at 28 dpl and 35 dpl compared with the non-lesioned group. However, $\lambda_\perp$ decreased in lesioned rats treated with β-CCB and was significantly different at 35 dpl compared with untreated lesioned animals and non-lesioned animals. Treatment with β-CCB in non-lesioned animals did not change $\lambda_\perp$ values significantly. On the other hand, $\lambda_{||}$ values did not show significant differences between the experimental groups.

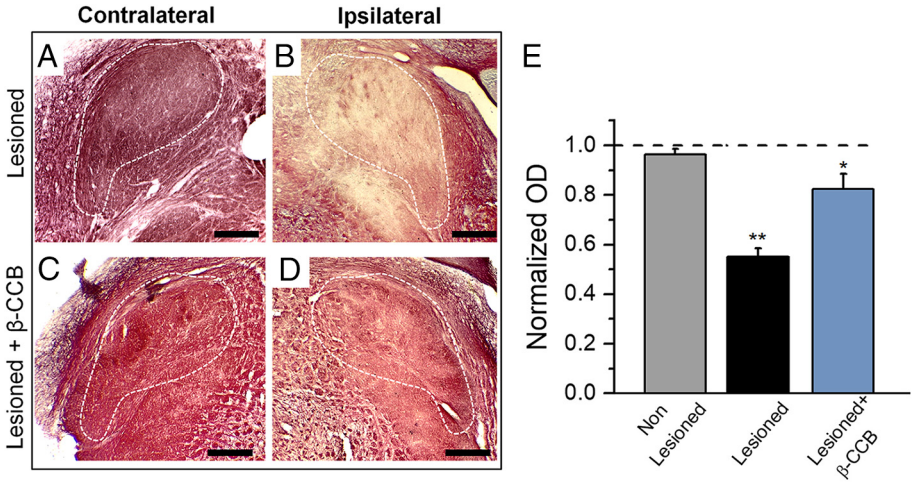

Fig. 4. Effect of β-CCB on the DRCCP model visualized by BGII staining. Images are representative coronal sections in the *c.c.p.* area (dotted line) stained with BGII to identify myelinated tracts; preparations were processed 35 days after EB injection in the *c.c.p.* Contralateral **(A and C)** sections correspond to the non-injected side, whereas ipsilateral **(B and D)** sections correspond to the injected side. A group of lesioned animals was i.p. injected with vehicle (A and B) every day from day 14 to day 28, and another group (C and D) was i.p. injected with β-CCB (1 mg/kg, under the same schedule as the vehicle). Bars = 500 μm. **(E)** Normalized optical density (OD) derived from BGII staining images. Columns show the ipsilateral optical density (mean ± S.E.M.) of the *c.c.p.* area in non-lesioned (n = 5), lesioned (n = 5), and β-CCB-treated lesioned (n = 5) animals, all normalized against the respective contralateral side (broken line). **Lesioned vs. Non-Lesioned ($P < 0.01$), *Lesioned + β-CCB vs. Lesioned ($P < 0.05$).

Finally, although the non-lesioned group showed constant FA, the non-lesioned group treated with β-CCB showed a tendency to increase FA at the end of the study (see Fig. 6A). Also, the contralateral FA values seemed to be higher in β-CCB–treated animals than in non-treated animals (Fig. 6B). This suggested that other tracts were affected by systemic β-CCB administration. To explore this possibility, we analyzed images of slices obtained from non-lesioned animals in both non-treated and β-CCB–treated groups. These slices included the corpus callosum (*c.c.*). The analysis was performed on days 0, 14 and 35 of treatment. The FA value for the *c.c.* significantly increased (10 ± 1.5%) on day 35 in the β-CCB-treated group compared with the basal FA on day 0 (before treatment) or compared with FA in the non-treated group on day 35 (Fig. 8). Treatment with β-CCB in non-lesioned animals also caused a significant change in $\lambda_{\perp}$ values on day 35; this parameter decreased by 12 ± 0.7% compared with the corresponding values on days 0 and 14 (Fig. 8D). However, $\lambda_{||}$ values did not show significant differences between groups at any time. These findings supported the idea that β-CCB treatment had a generalized effect on myelinated tracts as estimated from the MRI analysis.

DISCUSSION

Several injuries or pathologies in the CNS involve demyelination in the white and gray matter and axonal damage; for example, multiple sclerosis and diffuse white matter injury, which includes damage generated by hypoxic events during the neonatal period (Back, 2006; Trapp and Nave, 2008; Anjari et al., 2009; Saxena et al., 2011). The complex mechanisms and functional consequences of CNS demyelination and remyelination have yet to be fully understood; therefore, animal models have become useful to investigate the underlying mechanisms of these processes. *In vivo* models for white matter damage have been developed using demyelinating agents injected in specific CNS areas (Blakemore, 1974; Matute, 1998; Woodruff and Franklin, 1999; Gautier et al., 2015; Goudarzi et al., 2016) or by treatment with toxic agents administered systemically (Skripuletz et al., 2008; Manterola et al., 2018). A key goal for the development of such animal models is finding strategies to promote oligodendrocyte maturation and the subsequent remyelination. Thus, longitudinal studies to monitor de- and remyelination phenomena are of interest to evaluate both the potential effects of novel pharmacological or genetic strategies and the mechanisms involved. In this study we used MRI to quantify abnormalities in the DRCCP model and correlate these measures with histological alterations using the BGII technique.

Histological analysis showed a clear decrease in the optical density of staining of the *c.c.p.* that was EB-injected 35 days before. A direct correlation between the strength of staining (from red to brownish) using BGII and myelin content is supported by numerous studies (Chen et al., 2004; Schmued et al., 2008; Hakkarainen et al., 2016; Holleran et al., 2017; Yeh et al., 2017); thus, we infer that the decrease observed in the optical density in the EB-injected group indicated a decrease in myelin in the *c.c.p.* In the study by Woodruff and Franklin (1999), demyelinating lesions produced by EB-injection in the *c.c.p.* became clear around 14 dpl and lasted more than 3 months as studied by electron microscopy; hence, a decrease in myelin from 14 dpl to 35 dpl is in agreement with this study.

We applied longitudinal MRI analysis techniques that offer detailed information about the brain microstructure and function. The *c.c.p.* is especially suitable for this task because analysis is more robust in heavily myelinated tracts that lack crossings or interwoven paths. Our main goal was to explore whether the changes observed after the EB-induced lesion could be monitored using image analysis techniques. DTI analysis provides information about white matter microstructure in normal or pathological conditions (e.g., Song et al., 2005; Concha et al., 2006; Laitinen et al., 2010; Laitinen et al., 2015), and through FA calculation derived from DTI, this parameter reflects the coherent microscopic organization of axons. Thus, it is well known that an FA decrease correlates with lesioned white matter that might include both a decrease in myelin content and an increase of axonal damage (Song et al., 2002; Song et al., 2003; Kumar et al., 2009). Here we observed an FA

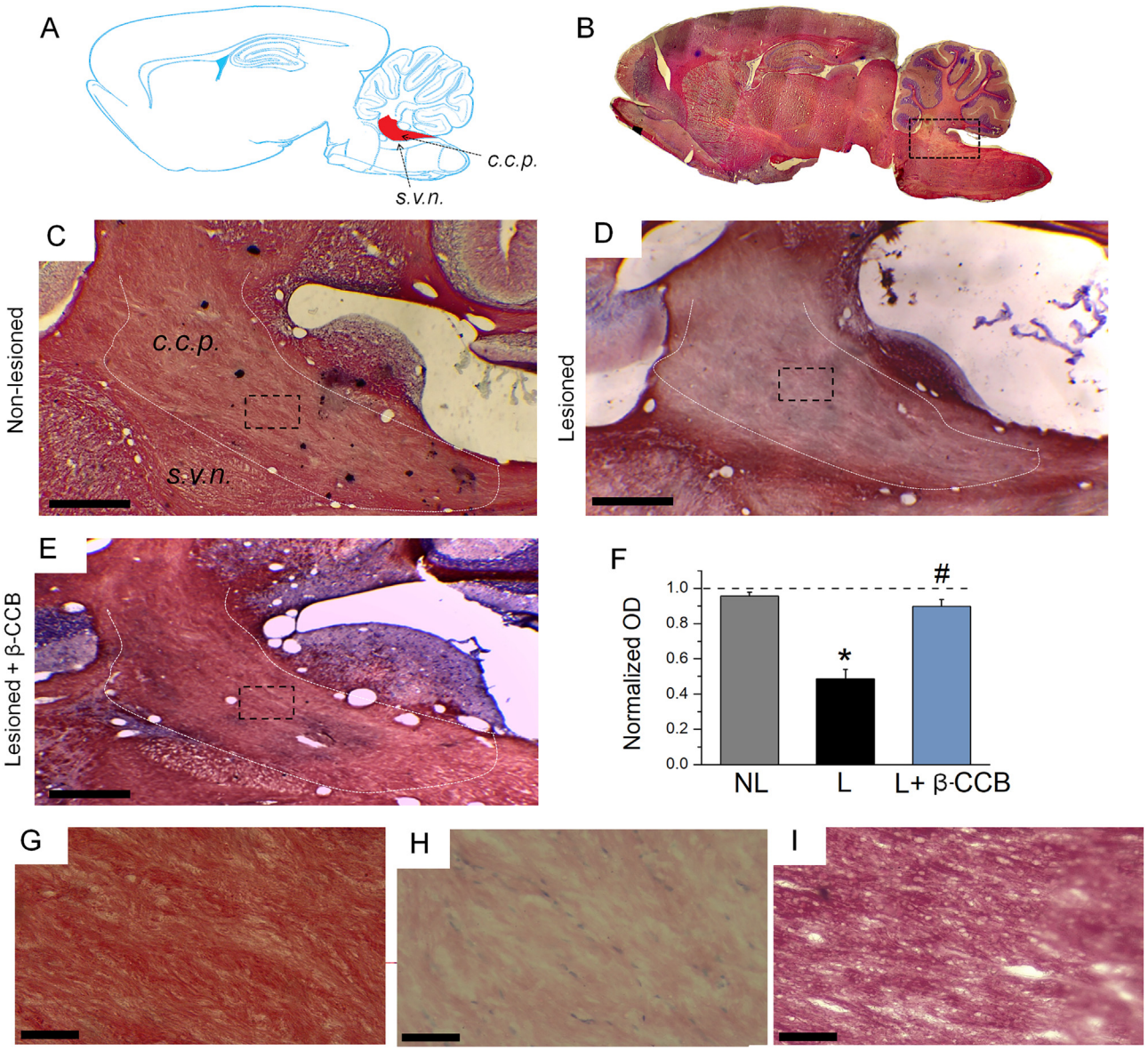

Fig. 5. Effect of β-CCB on the DRCCP model visualized by BGII staining. **(A)** Sagittal diagram of the brain illustrating the *c.c.p.* location signaled in red. **(B)** Sagittal section of the brain stained with BGII (*c.c.p.* area, dotted square) to identify myelinated tracts; preparations were processed 35 days after *c.c.p.* injection with either saline solution (non-lesioned) or EB (lesioned). The last group was subdivided into animals injected with vehicle or animals treated with β-CCB. **(C)** A representative non-lesioned *c.c.p.* (dotted line), **(D)** the *c.c.p.* of a lesioned animal without β-CCB treatment, **(E)** the *c.c.p.* of a lesioned animal treated with β-CCB (C–E, bars = 200 μm). **(G)**, **(H)** and **(I)** are amplified views (bars = 50 μm) of corresponding images signaled by black squares within the *c.c.p.* in panels C-E, respectively. **(F)** Columns illustrate the normalized OD (mean ± S.E.M.) derived from the BGII images in sagittal sections of the *c.c.p.* in non-lesioned (NL; $n = 4$) animals, as well as lesioned either without (L; $n = 5$) or with β-CCB treatment (L + β-CCB; $n = 6$). The *c.c.p.* ODs were normalized against the OD estimated in the respective spinal vestibular nucleus (*s.v.n.*; see A and C*)* area. *L vs. NL; $^{\#}$L + β-CCB vs. L ($P < 0.05$).

decrease in the *c.c.p.* of EB-injected animals scanned at 14 dpl. This decay, monitored every week, was sustained up to 35 dpl. Given that decreases in FA are a clear indicator of microstructure disarrangement, this result strongly suggests that a lesioned area was produced in EB-injected subjects. Thus, both BGII and MRI analysis supported the idea that the DRCCP model by EB injection produced a demyelinating *c.c.p.* lesion that can be longitudinally followed using image analysis.

The time-course analysis of this effect is essential to explore the actions of potential drugs and other therapeutic tools in the remyelination process, which has shown to occur several weeks later. Using BGII and MRI, we explored the possible effect of β-CCB administration; this β-carboline has been shown to have a potentiating effect on the $GABA_A$ response elicited in both OPCs and myelinating oligodendrocytes (Arellano et al., 2016). The effect of β-carbolines as positive modulators (and as inverse agonists) on $GABA_A$ receptors is not new (e.g., Thomet et al., 1999); however, we showed that β-CCB acts differentially, displaying a robust potentiating effect on the receptors expressed in OPCs, different from its negative or lack of effect on the response expressed in neurons. We used this differential pharmacologic outcome to study whether or not

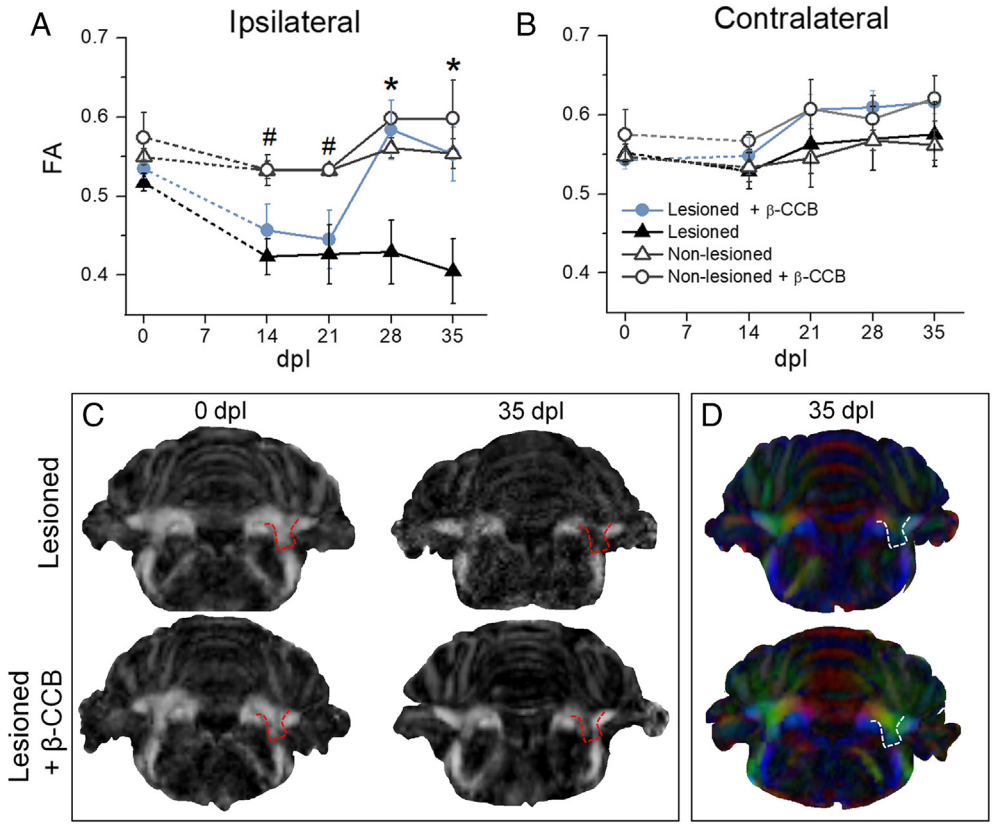

Fig. 6. FA analysis of the DRCCP model and the effect of β-CCB. FA quantification was performed for the *c.c.p.* area for both hemispheres, ipsilateral **(A)** and contralateral **(B)** to the lesion, and for the following four animal groups: lesioned (solid symbols) and non-lesioned animals (empty symbols), and animals with β-CCB treatment (circles; treatment schedule was the same as in Figs. 4 and 5) or without treatment (triangles). FA values were calculated from MRI; first, before the *c.c.p.* injection (0 dpl; with either control saline solution or EB) and then weekly from 14 dpl to 35 dpl (dotted line from 0 to 14 dpl indicates a time interval without MRI monitoring). Data are the mean ± S.E.M. (n = 4 animals for each case). **(C)** Representative FA maps at 0 dpl and 35 dpl in the group of lesioned animals without (top row) or with (bottom row) β-CCB treatment. **(D)** PDV maps at 35 dpl; the generated *c.c.p.* ROIs in C-D were drawn in the zone indicated by dotted lines. *Lesioned + β-CCB vs. Lesioned ($P < 0.05$); # Non-lesioned vs. Lesioned ($P < 0.05$).

systemically-administered β-CCB might have an effect related to myelination in the DRCCP model. The results strongly suggested that β-CCB had a clear potentiator effect on the parameters that indicate improvement of myelination. This conclusion is more direct from the histological analysis, given that BGII showed, at 35 dpl, an increase in stain intensity estimated as optical density in the lesioned group treated with β-CCB, comparing the ipsilateral and contralateral sides of the *c.c.p.* and also comparing the *c.c.p.* of the experimental group with that of the non-lesioned group. However, this observation lacks the time-course of the effect as well as the opportunity for objective quantification.

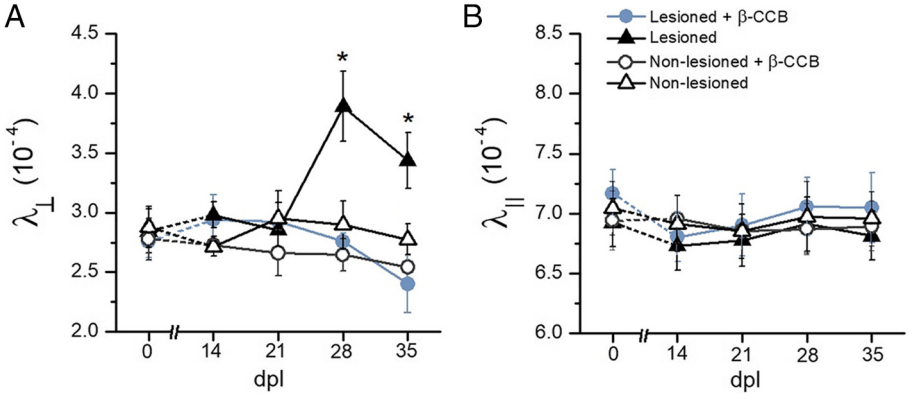

Fig. 7. Diffusivity (λ) during the DRCCP model and the β-CCB effect. Graphs depict the diffusivity values calculated from DTI for both radial ($\lambda_{\perp}$, in **A**) and axial ($\lambda_{||}$, in **B**) diffusivities, for images captured during the days indicated. Experimental groups are the same as those in Fig. 6A–B. *Lesioned + β-CCB vs. Lesioned in 28 and 35 dpl ($P < 0.05$); There was no statistically significant difference between Lesioned + β-CCB vs. Non-lesioned + β-CCB in 35 dpl; n = 4 for each case.

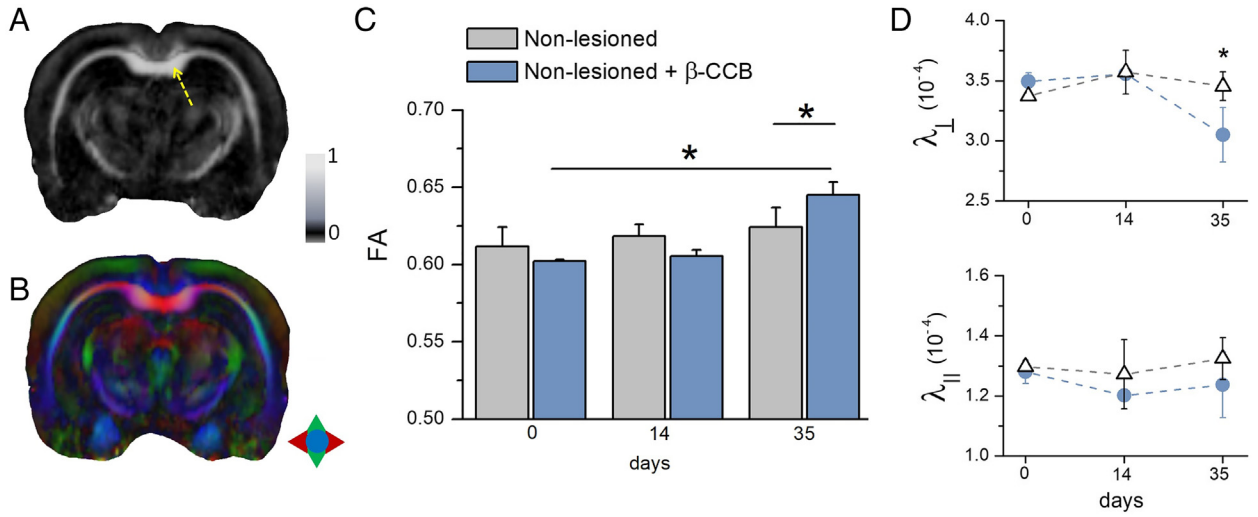

Fig. 8. β-CCB promoted FA increase in the *c.c.* of non-lesioned animals. **(A)** and **(B)** correspond to FA and PDV maps, respectively, in rat brain regions showing the corpus callosum (*c.c.*; yellow arrow in A). The PDV map was used to draw *c.c.* ROIs in order to calculate the corresponding FA values. **(C)** Columns represent the mean ± S.E.M. of FA for the *c.c.* in the non-lesioned groups either without or with β-CCB treatment, calculated at days 0, 14 and 35 after *c.c.p.* injection with saline (*P < 0.05). **(D)** Radial and axial diffusivities ($\lambda_{\perp}$ and $\lambda_{||}$) of *c.c.* before (0 day) and after the treatment with β-CCB (n = 4 for each case). *β-CCB-treated vs. non-treated (P < 0.05).

Longitudinal MRI analysis offsets these drawbacks and offers other advantages. DTI evaluation in lesioned rats showed an FA decrease analyzed at 14 dpl; this decrease was not observed in non-lesioned rats or in the contralateral *c.c.p.* of the lesioned subjects. The FA decrease in the untreated lesioned group was sustained at least until 35 dpl, the last day of analysis; whereas the non-lesioned group maintained the initial FA value throughout the study. In the lesioned β-CCB-treated group, a robust recovery of the FA value was observed at 28 dpl and 35 dpl, although FA improvement cannot be directly correlated with an increase in myelination. This result, together with BGII images at 35 dpl, seems to indicate that at least part of the FA recovery in the β-CCB group can be explained by an increase in the amount of myelin. The $\lambda_{\perp}$ decay in the lesioned β-CCB-treated group at 28 dpl and 35 dpl also suggested an improvement in myelination (Song et al., 2002; Song et al., 2003). At the same time, $\lambda_{||}$ did not show significant changes during the period of analysis in all groups, a result that is in agreement with reports suggesting low axonal damage by EB injection in the *c.c.p.* (Woodruff and Franklin, 1999).

Moreover, DTI metrics evaluation in the *c.c.* also showed that β-CCB administration promoted an increase in FA values, as well as a slight decrease in $\lambda_{\perp}$. This finding indicated that the effect of β-CCB might be generalized on other tracts. However, increased FA also has been seen in contexts not directly related to myelination improvement (Voss et al., 2006; Wilde et al., 2008; Lo et al., 2009; Budde et al., 2011). Thus, two basic aspects should be studied further: First, a possible myelin sheath recovery must be shown using ultrastructural techniques and/or molecular approaches; second, although myelination improvement might have some relation to the GABAergic signaling increase in the oligodendroglial lineage, the cellular mechanism involved in the effect of β-CCB remains unknown, and direct evidence for this relationship should be explored in detail.

In summary, these findings suggest that *c.c.p.* remyelination in the DRCCP model can be monitored longitudinally by MRI, measuring FA and λ values; and that β-CCB treatment improved the remyelination process. Therefore, they are useful for the development of animal models to perform quantitative longitudinal analyses of demyelination and remyelination processes and to test and validate novel therapeutic strategies.

ACKNOWLEDGMENTS

We thank Jessica González Norris for editing this manuscript. We also thank Felipe Cornejo Ortiz, Nydia Hernández Rios, Martín García Servín, Fernando Rodríguez, and Ramón Martínez Olvera for their expert technical support. We appreciate the important help of Dr. Isaac Silva during the initial experimental stage. This study was supported by grants from CONACYT-México No. 252121 and PAPIIT-UNAM-México No. IN203519 to R.O.A. laboratory. A.C-M is a researcher from Cátedras-CONACYT commissioned at Instituto de Neurobiología at Universidad Nacional Autónoma de México (UNAM).

This study is dedicated to the memory of our unforgettable Professor Ricardo Miledi. In many ways he was the instigator of questions contained in this work. He contributed with an amazing catalog of extraordinary original findings that are fundamental for understanding the complex intercellular communication mechanisms, a task that he considered the basis to understand the human brain, in his own words, the most stunning, significant, and universal frontier.

REFERENCES

Anjari M, Counsell SJ, Srinivasan L, Allsop JM, Hajnal JV, Rutherford MA, Edwards AD. (2009) The association of lung disease with cerebral white matter abnormalities in preterm infants. Pediatrics 124 (1):268-276, https://doi.org/10.1542/peds.2008-1294.

Arellano RO, Sánchez-Gómez MV, Alberdi E, Canedo-Antelo M, Chara JC, Palomino A, Pérez-Samartín A, Matute C. (2016) Axon-to-glia interaction regulates GABAA receptor expression in oligodendrocytes. Mol Pharmacol 89(1):63-74, https://doi.org/10.1124/mol.115.100594.

Arfanakis K, Haughton VM, Carew JD, Rogers BP, Dempsey RJ, Meyerand ME. (2002) Diffusion tensor MR imaging in diffuse axonal injury. AJNR Am J Neuroradiol 23(5):794-802.

Back SA. (2006) Perinatal white matter injury: the changing spectrum of pathology and emerging insights into pathogenetic mechanisms. Ment Retard Dev Disabil Res Rev 12:129-140, https://doi.org/10.1002/mrdd.20107.

Basser PJ, Mattiello J, LeBihan, D. . (1994) MR diffusion tensor spectroscopy and imaging. Biophys J 66(1):259-267, https://doi.org/10.1016/S0006-3495(94)80775-1.

Beaulieu C. (2002) The basis of anisotropic water diffusion in the nervous system–a technical review. NMR Biomed 15(7–8):435-455, https://doi.org/10.1002/nbm.782.

Blakemore WF. (1974) Remyelination of the superior cerebellar peduncle in old mice following demyelination induced by cuprizone. J Neurol Sci 22(1):121-126, https://doi.org/10.1016/0022-510X(74)90059-8.

Bora E, Harrison BJ, Fornito A, Cocchi L, Pujol J, Fontenelle LF, Velakoulis D, Pantelis C, Yücel M. (2011) White matter microstructure in patients with obsessive–compulsive disorder. J Psychiatry Neurosci 36(1):42, https://doi.org/10.1503/jpn.100082.

Boretius S, Escher A, Dallenga T, Wrzos C, Tammer R, Brück W, Nessler S, Frahm J, Stadelmann C. (2012) Assessment of lesion pathology in a new animal model of MS by multiparametric MRI and DTI. Neuroimage 59(3):2678-2688, https://doi.org/10.1016/j.neuroimage.2011.08.051.

Budde MD, Janes L, Gold E, Turtzo LC, Frank JA. (2011) The contribution of gliosis to diffusion tensor anisotropy and tractography following traumatic brain injury: validation in the rat using Fourier analysis of stained tissue sections. Brain 134(8):2248-2260, https://doi.org/10.1093/brain/awr161.

Cammer W, Zhang H. (1999) Atypical glial cells in demyelinated and hypomyelinated mouse brains. Brain Res 837:188-192, https://doi.org/10.1016/S0006-8993(99)01621-2.

Chen MK, Baidoo K, Verina T, Guilarte TR. (2004) Peripheral benzodiazepine receptor imaging in CNS demyelination: functional implications of anatomical and cellular localization. Brain 127(6):1379-1392, https://doi.org/10.1093/brain/awh161.

Concha L. (2014) A macroscopic view of microstructure: using diffusion-weighted images to infer damage, repair, and plasticity of white matter. Neuroscience 276:14-28, https://doi.org/10.1016/j.neuroscience.2013.09.004.

Concha L, Gross DW, Wheatley BM, Beaulieu C. (2006) Diffusion tensor imaging of time-dependent axonal and myelin degradation after corpus callosotomy in epilepsy patients. Neuroimage 32(3):1090-1099, https://doi.org/10.1016/j.neuroimage.2006.04.187.

Dal Canto MC, Melvold RW, Kim BS, Miller SD. (1995) Two models of multiple sclerosis: experimental allergic encephalomyelitis (EAE) and Theiler's murine encephalomyelitis virus (TMEV) infection. A pathological and immunological comparison. Microsc Res Tech 32(3):215-229, https://doi.org/10.1002/jemt.1070320305.

De Stefano N, Narayanan S, Francis GS, Arnaoutelis R, Tartaglia MC, Antel JP, Matthews PM, Arnold DL. (2001) Evidence of axonal damage in the early stages of multiple sclerosis and its relevance to disability. Arch Neurol 58(1):65-70, https://doi.org/10.1001/archneur.58.1.65.

Fancy SP, Zhao C, Franklin RJ. (2004) Increased expression of Nkx2. 2 and Olig2 identifies reactive oligodendrocyte progenitor cells responding to demyelination in the adult CNS. Mol Cell Neurosci 27(3):247-254, https://doi.org/10.1016/j.mcn.2004.06.015.

Fancy SPJ, Chan JR, Baranzini SE, Franklin RJM, Rowitch DH. (2011) Myelin regeneration: a recapitulation of development? Annu Rev Neurosci 34:21-43, https://doi.org/10.1146/annurev-neuro-061010-113629.

Farzin D, Mansouri N. (2006) Antidepressant-like effect of harmane and other B-carbolines in the mouse forced swim test. Neuropsychoph Journal 11:126, https://doi.org/10.1016/j.euroneuro.2005.08.005.

Fatemi SH, Folsom TD, Reutiman TJ, Abu-Odeh D, Mori S, Huang H, Oishi K. (2009) Abnormal expression of myelination genes and alterations in white matter fractional anisotropy following prenatal viral influenza infection at E16 in mice. Schizophr Res 112(1–3):46-53, https://doi.org/10.1016/j.schres.2009.04.014.

Gautier HO, Evans KA, Volbracht K, James R, Sitnikov S, Lundgaard I, James F, Lao-Peregrin C, et al. (2015) Neuronal activity regulates remyelination via glutamate signaling to oligodendrocyte progenitors. Nat Commun 6:8518, https://doi.org/10.1038/ncomms9518.

Godfraind C, Friedrich VL, Holmes KV, Dubois-Dalcq M. (1989) In vivo analysis of glial cell phenotypes during a viral demyelinating disease in mice. J Cell Biol 109(5):2405-2416, https://doi.org/10.1083/jcb.109.5.2405.

Goudarzi S, Rivera A, Butt AM, Hafizi S. (2016) Gas6 promotes oligodendrogenesis and myelination in the adult central nervous system and after lysolecithin-induced demyelination. ASN Neuro 2016:8, https://doi.org/10.1177/1759091416668430.

Grella B, Dukat M, Young R, Teitler M, Herrick-Davis K, Gauthier CB, Glennon RA. (1998) Investigation of hallucinogenic and related β-carbolines. Drug Alcohol Depend 50(2):99-107, https://doi.org/10.1016/S0376-8716(97)00163-4.

Hakkarainen H, Sierra A, Mangia S, Garwood M, Michaeli S, Gröhn O, Liimatainen T. (2016) MRI relaxation in the presence of fictitious fields correlates with myelin content in normal rat brain. Magn Reson Med 75(1):161-168, https://doi.org/10.1002/mrm.25590.

Hamilton NB, Clarke LE, Arancibia-Carcamo IL, Kougioumtzidou E, Matthey M, Káradóttir R, Whiteley L, Bergersen LH, Attwell D. (2017) Endogenous GABA controls oligodendrocyte lineage cell number, myelination, and CNS internode length. Glia 65(2):309-321, https://doi.org/10.1002/glia.23093.

Holleran L, Kim JH, Gangolli M, Stein T, Alvarez V, McKee A, Brody DL. (2017) Axonal disruption in white matter underlying cortical sulcus tau pathology in chronic traumatic encephalopathy. Acta Neuropathol 133(3):367-380, https://doi.org/10.1007/s00401-017-1686-x.

Kassmann CM, Nave KA. (2008) Oligodendroglial impact on axonal function and survival – a hypothesis. Curr Opin Neurol 21(3):235-241.

Kumar R, Husain M, Gupta RK, Hasan KM, Haris M, Agarwal AK, Pandey CM, Narayana PA. (2009) Serial changes in the white matter diffusion tensor imaging metrics in moderate traumatic brain injury and correlation with neuro-cognitive function. J Neurotrauma 26(4):481-495, https://doi.org/10.1089/neu.2008.0461.

Kutzelnigg A, Lucchinetti CF, Stadelmann C, Brück W, Rauschka H, Bergmann M, Schmidbauer M, Parisi JE, Lassmann H. (2005) Cortical demyelination and diffuse white matter injury in multiple sclerosis. Brain 128(11):2705-2712, https://doi.org/10.1093/brain/awh641.

Laitinen T, Sierra A, Pitkänen A, Gröhn O. (2010) Diffusion tensor MRI of axonal plasticity in the rat hippocampus. Neuroimage 51(2):521-530, https://doi.org/10.1016/j.neuroimage.2010.02.077.

Laitinen T, Sierra A, Bolkvadze T, Pitkänen A, Gröhn O. (2015) Diffusion tensor imaging detects chronic microstructural changes in white and gray matter after traumatic brain injury in rat. Front Neurosci 9:128, https://doi.org/10.3389/fnins.2015.00128.

Larm JA, Cheung NS, Beart PM. (1996) (S)-5-fluorowillardiine-mediated neurotoxicity in cultured murine cortical neurons occurs via AMPA and kainate receptors. Eur J Pharmacol 314(1–2):249-254, https://doi.org/10.1016/S0014-2999(96)00633-4.

Larvaron P, Boespflug-Tanguy O, Renou JP, Bonny JM. (2007) In vivo analysis of the post-natal development of normal mouse brain by DTI. NMR Biomed 20(4):413-421, https://doi.org/10.1002/nbm.1082.

Li Q, Sun J, Guo L, Zang Y, Feng Z, Huang X, Yang H, Lv Y, Huang M, Gong Q. (2010) Increased fractional anisotropy in white matter of the right frontal region in children with attention-deficit/hyperactivity disorder: a diffusion tensor imaging study. Neuroendocrinol Lett 31(6):747, https://doi.org/10.1007/s00787-010-0113-9.

Lo C, Shifteh K, Gold T, Bello JA, Lipton ML. (2009) Diffusion tensor imaging abnormalities in patients with mild traumatic brain injury and neurocognitive impairment. J Comput Assist Tomogr 33(2):293-297, https://doi.org/10.1097/RCT.0b013e31817579d1.

Manterola A, Bernal-Chico A, Cipriani R, Canedo-Antelo M, Moreno-García Á, Martín-Fontecha M, Pérez-Cerda F, Sánchez-Gómez

MV, et al. (2018) Deregulation of the endocannabinoid system and therapeutic potential of ABHD6 blockade in the cuprizone model of demyelination. Biochem Pharmacol 157:189-201, https://doi.org/10.1016/j.bcp.2018.07.042.

Matute C. (1998) Characteristics of acute and chronic kainate excitotoxic damage to the optic nerve. PNAS 95(17):10229-10234, https://doi.org/10.1073/pnas.95.17.10229.

McCarthy KD, De Vellis J. (1980) Preparation of separate astroglial and oligodendroglial cell cultures from rat cerebral tissue. J Cell Biol 85:890-902, https://doi.org/10.1083/jcb.85.3.890.

McGavern DB, Murray PD, Rodriguez M. (1999) Quantitation of spinal cord demyelination, remyelination, atrophy, and axonal loss in a model of progressive neurologic injury. J Neurosci Res 58(4):492-504, https://doi.org/10.1002/(SICI)1097-4547(19991115)58:4<492::AID-JNR3>3.0.CO;2-P.

Meeson AP, Piddlesden S, Morgan BP, Reynolds R. (1994) The distribution of inflammatory demyelinated lesions in the central nervous system of rats with antibody-augmented demyelinating experimental allergic encephalomyelitis. Exp Neurol 129:299-310, https://doi.org/10.1006/exnr.1994.1172.

Miller DJ, Rodriguez M. (1996) Spontaneous central nervous system remyelination in strain a mice after infection with the Daniel's (DA) strain of Theiler's virus. Acta Neuropathol (Berl) 91(6):559-565, https://doi.org/10.1007/s004010050.

Paxinos G, Watson C. (2007) The rat brain in stereotaxic coordinates. New York, NY: Academic Press, 2007.

Peña C, Medina JH, Novas ML, Paladini AC, De Robertis E. (1986) Isolation and identification in bovine cerebral cortex of n-butyl beta-carboline-3-carboxylate, a potent benzodiazepine binding inhibitor. PNAS 83(13):4952-4956, https://doi.org/10.1073/pnas.83.13.4952.

Pérez-Samartín A, Garay E, Moctezuma JPH, Cisneros-Mejorado A, Sánchez-Gómez MV, Martel-Gallegos G, Robles-Martínez L, Canedo-Antelo M, et al. (2017) Inwardly rectifying K+ currents in cultured oligodendrocytes from rat optic nerve are insensitive to pH. Neurochem Res 42(9):2443-2455, https://doi.org/10.1007/s11064-017-2242-8.

Perry VH, Anthony DC. (1999) Axon damage and repair in multiple sclerosis. Philos Trans R Soc Lond B Biol Sci 354:1641-1647, https://doi.org/10.1098/rstb.1999.0509.

Raine CS, Snyder DH, Valsamis MP, Stone SH. (1974) Chronic experimental allergic encephalomyelitis in inbred guinea pigs. An ultrastructural study. Lab Invest 31:369-380.

Rodríguez-Cruces R, Velázquez-Pérez L, Rodríguez-Leyva I, Velasco AL, Trejo-Martínez D, Barragán-Campos HM, Camacho-Tellez V, Concha L. (2018) Association of white matter diffusion characteristics and cognitive deficits in temporal lobe epilepsy. Epilepsy & Behav 79:138-145, https://doi.org/10.1016/j.yebeh.2017.11.040.

Sánchez-Gómez MV, Serrano MP, Alberdi E, Pérez-Cerdá F, Matute C. (2018) Isolation, expansion, and maturation of oligodendrocyte lineage cells obtained from rat neonatal brain and optic nerve. In Myelin (pp. 95–113). New York, NY: Humana Press, 2018 https://doi.org/10.1007/978-1-4939-7862-5_8.

Sasaki M, Ide C. (1989) Demyelination and remyelination in the dorsal funiculus of the rat spinal cord after heat injury. J Neurocytol 18:225-239, https://doi.org/10.1007/BF01206664.

Saxena A, Martin-Blondel G, Mars LT, Liblau RS. (2011) Role of CD8 T cell subsets in the pathogenesis of multiple sclerosis. FEBS Lett 585 (23):3758-3763, https://doi.org/10.1016/j.febslet.2011.08.047.

Schmued L, Bowyer J, Cozart M, Heard D, Binienda Z, Paule M. (2008) Introducing Black–Gold II, a highly soluble gold phosphate complex with several unique advantages for the histochemical localization of myelin. Brain Res 1229:210-217, https://doi.org/10.1016/j.brainres.2008.06.129.

Schmued LC. (1990) A rapid, sensitive histochemical stain for myelin in frozen brain sections. J Histochem Cytochem 38(5):717-720, https://doi.org/10.1177/38.5.1692056.

Skripuletz T, Lindner M, Kotsiari A, Garde N, Fokuhl J, Linsmeier F, Trebst C, Stangel M. (2008) Cortical demyelination is prominent in the murine cuprizone model and is strain-dependent. Am J Pathol 172(4):1053-1061, https://doi.org/10.2353/ajpath.2008.070850.

Song SK, Sun SW, Ramsbottom MJ, Chang C, Russell J, Cross AH. (2002) Dysmyelination revealed through MRI as increased radial (but unchanged axial) diffusion of water. Neuroimage 17(3):1429-1436, https://doi.org/10.1006/nimg.2002.1267.

Song SK, Sun SW, Ju WK, Lin SJ, Cross AH, Neufeld AH. (2003) Diffusion tensor imaging detects and differentiates axon and myelin degeneration in mouse optic nerve after retinal ischemia. Neuroimage 20 (3):1714-1722, https://doi.org/10.1016/j.neuroimage.2003.07.005.

Song SK, Yoshino J, Le TQ, Lin SJ, Sun SW, Cross AH, Armstrong RC. (2005) Demyelination increases radial diffusivity in corpus callosum of mouse brain. Neuroimage 26(1):132-140, https://doi.org/10.1016/j.neuroimage.2005.01.028.

Stricker NH, Schweinsburg BC, Delano-Wood L, Wierenga CE, Bangen KJ, Haaland KY, Frank LR, Salmon DP, Bondi MW. (2009) Decreased white matter integrity in late-myelinating fiber pathways in Alzheimer's disease supports retrogenesis. Neuroimage 45 (1):10-16, https://doi.org/10.1016/j.neuroimage.2008.11.027.

Thomet U, Baur R, Scholze P, Sieghart W, Sigel E. (1999) Dual mode of stimulation by the β-carboline ZK 91085 of recombinant GABAA receptor currents: molecular determinants affecting its action. Br J Pharmacol 127(5):1231-1239, https://doi.org/10.1038/sj.bjp.0702639.

Trapp BD, Nave KA. (2008) Multiple sclerosis: an immune or neurodegenerative disorder? Annu Rev Neurosci 31:247-269, https://doi.org/10.1146/annurev.neuro.30.051606.094313.

Trapp BD, Ransohoff R, Rudick R. (1999) Axonal pathology in multiple sclerosis: relationship to neurologic disability. Curr Opin Neurol 12 (3):295-302.

Van der Valk P, De Groot CJA. (2000) Staging of multiple sclerosis (MS) lesions: pathology of the time frame of MS. Neuropathol Appl Neurobiol 26:2-10, https://doi.org/10.1046/j.1365-2990.2000.00217.x.

Veraart J, Fieremans E, Novikov DS. (2016) Diffusion MRI noise mapping using random matrix theory. Magn Reson Med 76(5):1582-1593, https://doi.org/10.1002/mrm.26059.

Voss HU, Uluç AM, Dyke JP, Watts R, Kobylarz EJ, McCandliss BD, Heier LA, Beattie BJ, et al. (2006) Possible axonal regrowth in late recovery from the minimally conscious state. J Clin Invest 2006 (116):2005-2011, https://doi.org/10.1172/JCI27021.

Wilde EA, McCauley SR, Hunter JV, Bigler ED, Chu Z, Wang ZJ, Hanten GR, Troyanskaya M, et al. (2008) Diffusion tensor imaging of acute mild traumatic brain injury in adolescents. Neurology 70(12):948-955, https://doi.org/10.1212/01.wnl.0000305961.68029.54.

Wolswijk G. (1998) Chronic stage multiple sclerosis lesions contain a relatively quiescent population of oligodendrocyte precursor cells. J Neurosci 18:601-609, https://doi.org/10.1523/JNEUROSCI.18-02-00601.1998.

Woodruff RH, Franklin RJM. (1999) Demyelination and remyelination of the caudal cerebellar peduncle of adult rats following stereotaxic injections of lysolecithin, ethidium bromide, and complement/anti-galactocerebroside: a comparative study. Glia 25:216-228, https://doi.org/10.1002/(SICI)1098-1136(19990201)25:3<216::AID-GLIA2>3.0.CO;2-L.

Yeh TY, Wang SM, Tseng GF, Liu PH. (2017) Differential regulation of glial reactions in the central facial tract and the facial nucleus after facial neurorrhaphy. J Chem Neuroanat 79:38-50, https://doi.org/10.1016/j.jchemneu.2016.11.005.

Yurgelun-Todd DA, Silveri MM, Gruber SA, Rohan ML, Pimentel PJ. (2007) White matter abnormalities observed in bipolar disorder: a diffusion tensor imaging study. Bipolar Disord 9(5):504-512, https://doi.org/10.1111/j.1399-5618.2007.00395.x.

Zhao C, Fancy SP, Franklin RJ. (2008) Osteopontin is extensively expressed by macrophages following CNS demyelination but has a redundant role in remyelination. Neurobiol Dis 31(2):209-217, https://doi.org/10.1016/j.nbd.2008.04.007.

Zonouzi M, Scafidi J, Li P, McEllin B, Edwards J, Dupree JL, Harvewy L, Sun D, et al. (2015) GABAergic regulation of cerebellar NG2 cell development is altered in perinatal white matter injury. Nature Neurosci 18(5):674, https://doi.org/10.1038/nn.3990.

(Received 21 March 2019, Accepted 28 June 2019)
(Available online xxxx)